

28 GHz Multi-User Massive Distributed-MIMO with Spatial Division Multiplexing

TAWA Noriaki, KUWABARA Toshihide, MARUTA Yasushi, KANEKO Tomoya

Abstract

This paper describes the experimental verifications of a 28 GHz multi-user massive distributed multiple-input multiple-output (MIMO) using comprehensive calibration without an additional transceiver path. A conventional massive collocated-MIMO using millimeter wave has low robustness in non-line of sight environments and restricts the number of simultaneously connected users due to the lack of propagation independent. The newly developed distributed MIMO system consists of the eight distributed active antennas connected to a digital and mixed signal processing unit. The proposed calibration for the distributed MIMO improves the pre-coding accuracy and enhances the number of simultaneously connected users and cell throughput. We demonstrate zero-forcing spatial multiplexing using up-link to down-link channel reciprocity for two, four, and six user equipment in an actual over-the-air office environment. The distributed MIMO shows high robustness in non-line of sight environments and a system throughput of 2.1 Gbps per 100 MHz for the sum of six simultaneous users.

Keywords



Beyond 5G and 6G mobile communications, MIMO, millimeter wave communication, propagation, space division multiplexing

1. Introduction

The beyond 5th and 6th generation mobile access services eager spatial division multiplexing (SDM) technologies by using massive multiple-input multiple-output (MIMO) systems to increase cell throughput and the number of simultaneously connected users. Furthermore, the benefits of using millimeter wave is cell throughput enhancement due to the wide available frequency range. The massive MIMO has two beam forming methods, which are analog and digital beam forming. Although analog beam forming can realize a few analog-to-digital converters (ADCs) and digital-to-analog converters (DACs), it restricts the number of accesses and cell throughput due to without null forming. In contrast, digital beam forming controls amplitude and phase of signals digitally, and enhances cell throughput by using null forming. However, digital beam forming using millimeter wave is constrained by various barriers, such as a limited number of effective multipath due to straightness, shadowing, and loss in propagations.

A collocated MIMO (C-MIMO) system is one of the implementation technique in massive MIMO, which lines up

multiple antenna elements with about half wave length spacing in a system. In contrast, a distributed MIMO (D-MIMO) technique ensures the individual effective multipath to maximize the performance of SDM by geometrically distant multiple number of antennas¹⁾⁻⁴⁾.

This paper describes the design and implementation of a 28 GHz D-MIMO radio unit (RU) and a newly developed comprehensive calibration over the distributed antennas, and demonstrates the up-link (UL) to down-link (DL) channel reciprocity with simultaneous multiple user connections in over the air (OTA) measurements.

2. 28 GHz D-MIMO Testbed

We developed a 28 GHz D-MIMO testbed that consists of a UL and DL mixed signal processing (MSP) unit and eight distributed antenna (DA) units. **Fig. 1** shows the block diagram of the AP D-MIMO testbed. **Table** shows its specifications.

MSP has a field-programmable array of Xilinx ZU29DR integrated with eight ADCs and eight DACs. The DACs directly generate TX intermediate frequency (IF) signals, and the ADCs directly receives RX IF signals. MSP and

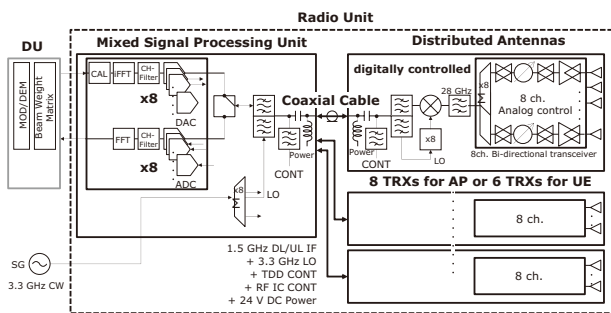


Fig. 1 Block diagram of the D-MIMO testbed.

Table Specifications of the D-MIMO testbed.

Parameters	Values	
Radio frequency	28.25 GHz	
Modulation scheme	OFDM	
Subcarrier spacing	60 kHz	
Signal bandwidth	80 MHz	
EIRP	22 dBm	
Noise figure	8 dB	
Number of DAs	8	
Number of antenna elements	per DA	AP total
	8	64

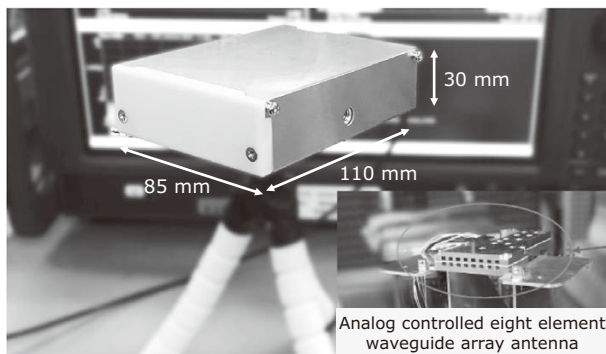


Fig. 2 Photos of DA and eight elements waveguide array antenna.

DAs have newly de-signed sextuple multiplexers, which multiple a TX IF signal, a RX IF signal, a 3.3 GHz local oscillator (LO) signal, a time division duplex control signal, a radio frequency (RF) integrated circuit (IC) control signal, and 24 V direct current power. The frequency of TX and RX IF signals is 1.5 GHz to decrease cable losses. Thus, each DA can be connected to MSP with a 20 m single coaxial cable and is located to an arbitrary place within the cable length.

DA has an 8-element waveguide array antenna with a half wave length element spacing at 28 GHz as shown in Fig. 2. The eight antenna elements connect to the eight

channel bi-directional transceiver IC based on 65 nm CMOS integrating gain and phase shifters⁵⁾. DA converts between the IF signals and 28.25 GHz RF signals by mixing with a LO signal generated by eight times of the original 3.3 GHz signal. The effective isotropic radiated power (EIRP) of the DA TX signal is 22 dBm.

A distributed unit (DU) generates digital baseband signals pre-coded with DL beam weights. The DL and UL signals are modulated with orthogonal frequency division multiplexing (OFDM), whose numerology is based on the specifications of 3GPP TS 36.211 format⁶⁾ except for sub-carrier spacing and signal bandwidth.

3. Calibration for D-MIMO

Transceivers in a conventional MIMO such as C-MIMO are calibrated so that the phase and amplitude are absolutely the same between the all transceivers. The calibration is called absolute calibration. For the absolute calibration, the conventional MIMO has a built-in calibration path to observe RF signals⁷⁾, and performs the absolute calibration in factory and on-site.

In contrast, the D-MIMO system does not perform the absolute calibration because the calibration path cannot be built in the RU due to the separated DAs. Furthermore, factory calibration is not sufficient enough for the efficient beam forming because the phase and amplitude of D-MIMO signal are varied by the length and forming of the coaxial cable between MSP and DA.

In this work, we propose a new calibration method that can be applicable to D-MIMO and realizes sufficient DL SDM quality. The calibration measures DL and UL calibration signals with OTA transmission by using an external probe antenna as shown in Fig. 3. Calibration signals are based on Zadoff-Chu sequence and are allocated to different subcarriers for each DA to prevent

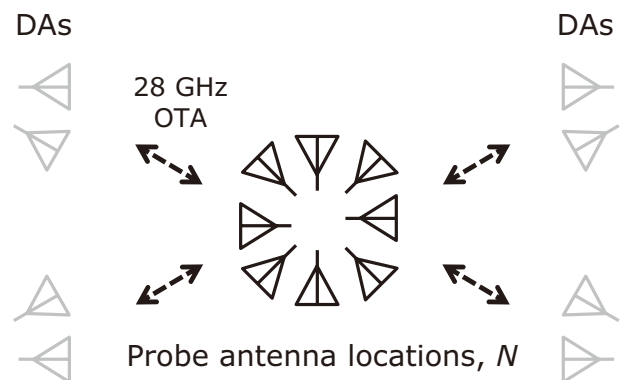


Fig. 3 Antenna locations for the D-MIMO calibration on the office floor.

interferences. The calibration signals are measured several times N at different locations and directions of the probe antenna to calibrate the all DAs.

The DL channel coefficient estimated from the calibration measurements between the k -th probe antenna location and the i -th DA, called DA- i , is expressed as follows,

$$h_{dl,k,i} = h_{k,i}g_{tx,i}, \quad (1)$$

where $h_{k,i}$ is the actual propagation channel from DA- i to the k -th probe antenna, $g_{tx,i}$ is the complex transmitter gain of DA- i , $k = 0, 1, \dots, N$, and $i = 0, 1, \dots, 8$. Similarly, the UL channel coefficient is expressed as,

$$h_{ul,k,i} = h_{k,i}g_{rx,i}, \quad (2)$$

where $g_{rx,i}$ is the complex receiver gain of DA- i . The calibration parameter for DA- i is calculated as follows,

$$c_i = \frac{\sum_{k=0}^{N-1} h_{ul,k,i} h_{dl,k,i}^*}{\sum_{k=0}^{N-1} |h_{dl,k,i}|^2}, \quad (3)$$

The symbol* denotes complex conjugate. (3) means the weighted average of the gain ratio, $g_{rx,i} / g_{tx,i}$, with the propagation attenuation. The weighted average improves accuracy of the calibration because the contribution of largely attenuated calibration signals, which have large noise, is decreased. The calibration parameter is obtained for each frequency of the subcarrier having the calibration signal, and is multiplied by the TX time-frequency domain OFDM signal.

In this measurement, the probe antenna is allocated to the approximately center of the communication area and is redirected in eight directions, $N = 8$, as shown in Fig. 3. Although the external probe antenna is used in this measurement, one of DAs can be used as a probe antenna for self-calibration⁸⁾.

4. Over-the-Air Measurements

Fig. 4 shows the DA and user equipment (UE) locations on an actual office floor. The UEs have the same architecture as the AP D-MIMO system. We evaluate the UL to DL channel reciprocity by changing the number of UEs connected simultaneously and with the same frequency. The number of UEs is two, four, and six, and each UE has single layer transmission.

The solid arrows and the dashed arrows show the antenna directions and locations of DAs and UEs, respectively. The directions of UE-0 from Desk-1 to Desk-15 are right, and the others are left.

4.1 Measurement Setup and Procedure

In the measurements, two of the eight DAs are located in each of the four corners in the communication area as shown in Fig. 4. The height of DA is about 1.7 m from

the floor.

Up to six UEs, UE-0 to UE-5, are allocated on the desks, and their heights are about 1.7 m from the floor. The UE-0 to UE-1 and the UE-0 to UE-3 are used for two and four UE multiplexing, respectively. The UE-0 is swept from the Desk-1 to Desk-27 to evaluate the multi-user channel reciprocity over the entire measurement area, and the other UEs are fixed to the locations on the desks shown in Fig. 4.

Firstly, AP D-MIMO receives UL signals from UEs and obtains channel coefficients. Subsequently, pre-coding weights are calculated by zero-forcing (ZF) method using the UL channels coefficients and are multiplied by the DL signals in DU. The DL signals use quadrature phase shift keying. The EVM for each UE is measured from the DL signal received through OTA transmission. The EVM measurement is repeated each time the UE-0 moves from Desk-1 to Desk-27 shown in Fig. 4.

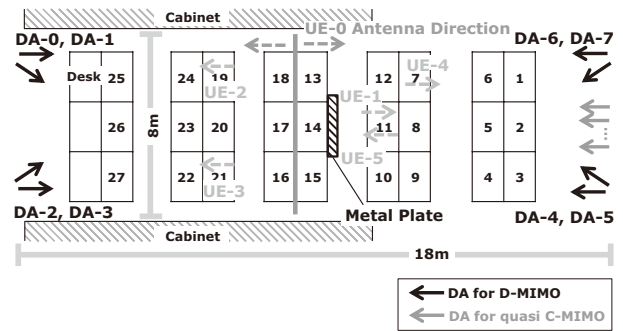
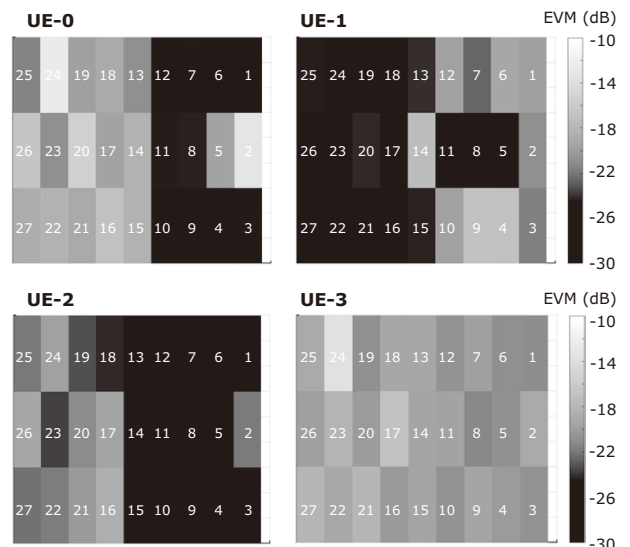


Fig. 4 Measurement layout on the office floor.



*Each cell number corresponds to the desk number in Fig. 4.

Fig. 5 EVM heat maps for four UE connection.

4.2 Measurement Results

Fig. 5 shows the heat maps of DL EVMs with four UEs connected simultaneously. Each cell in the heat map corresponds to the UE-0 location from Desk-1 to Desk-27 and represents the measured EVM for each UE. Although EVM degrades in some locations, EVM is lower than about -20 dB in most locations.

In the previous work, a D-MIMO testbed calibrated at the center frequency only has the EVM of -14 dB with two UEs connection and degrades the EVM according to the signal bandwidth¹⁾. EVM of this work is better than that of the previous work because the newly developed calibration can corrects the phase and amplitude frequency dependencies of DAs.

Fig. 6 shows system throughput (STP) as a function of the number of simultaneously connected UEs. STP is the total throughput of all UEs, and is estimated from the measured EVM, assuming the use of 5G New Radio signals with 100 MHz bandwidth⁹⁾. The circle dark gray and circle light gray lines in Fig. 6 show STP of the D-MIMO measurements with and without the metal plate shown in Fig. 4, respectively. STP with the plate is slightly higher than that without the plate, which implies that the signal contamination decreases due to the plate.

To compare D-MIMO and C-MIMO, STP is measured by the D-MIMO testbed lining up the eight DAs at 3 cm intervals as shown by the dark gray arrows in Fig. 4. Although a general C-MIMO has an antenna spacing of about a half wave length at the radio frequency, DAs cannot be arranged with a half wave length of 28 GHz due to the DA width of 3 cm. Thus, the testbed having these DA locations is called quasi C-MIMO. As shown

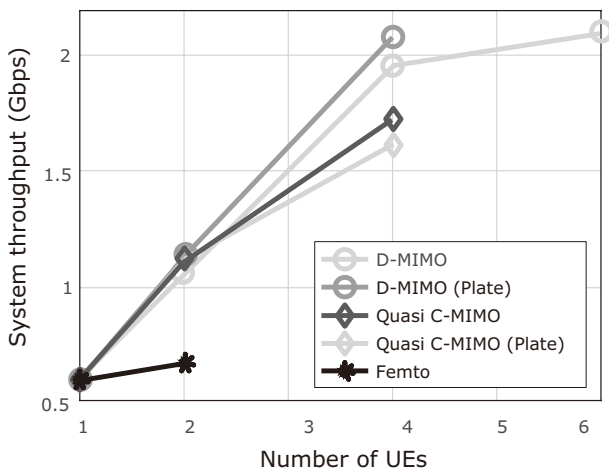


Fig. 6 System throughput estimated from the D-MIMO OTA experiment.

in Fig. 6, STP of quasi C-MIMO with the metal plate is less than that without the plate due to non-line of sight transmission.

Additionally, we investigate STP for femto-cell base stations. DA is assumed as a femto-cell base station and is connected to a single UE without using SDM in this measurement. UE-0 and UE-1 connect to DA-1 and DA-5, respectively. The black line in Fig. 6 shows STP of femto-cell base stations. STP for two UE connection is almost equivalent to STP for single UE connection due to signal contamination.

5. Conclusion

This paper has presented the experimental investigation of the AP 28 GHz multi-user D-MIMO using newly developed calibration. D-MIMO achieves STP of 2.1 Gbps per 100 MHz with six simultaneous connection and demonstrates higher STP than quasi C-MIMO and the femto-cell base stations. Additionally, the experimental investigation show that D-MIMO has high robustness in non-line of sight environments.

In conventional C-MIMO, the ratio $K/M = 1/4$, where the number of UEs is K , and the number of transceivers in the AP is M , is the preferred operating regime for multi-user MIMO⁷⁾¹⁰⁾. In contrast, the D-MIMO system shows that $K/M = 1/2$ is the available regime with sufficient throughput for each UE as shown in Fig. 6.

These findings suggest the potential for improving the cell throughput of the beyond 5th and 6th generation millimeter-wave services in indoor and densely populated outdoor areas with obstacles and pedestrians.

6. Acknowledgement

We would like to thank Professor Kenichi Okada and his laboratory's researchers at Tokyo Institute of Technology for their core chips prototyping and technical discussion.

References

- 1) N. Tawa, T. Kuwabara, Y. Maruta and T. Kaneko: Measuring Propagation Channel Variations and Reciprocity using 28 GHz Indoor Distributed Multi-user MIMO, 2020 IEEE Radio and Wireless Symposium (RWS formerly RAWCON), pp.104-107, January 2020
<https://ieeexplore.ieee.org/document/9050046>
- 2) N. Tawa, T. Kuwabara, Y. Maruta and T. Kaneko: 28 GHz Distributed-MIMO Comprehensive Antenna Calibration for 5G Indoor Spatial Division Multiplex, 2021 IEEE MTT-S International Microwave Symposium (IMS), pp.541-544, June 2021
<https://ieeexplore.ieee.org/document/9574898>
- 3) I. C. Sezgin, M. Dahlgren, T. Eriksson, M. Coldrey, C. Larsson, J. Gustavsson, and C. Fager: A Low-Complexity Distributed-MIMO Testbed Based on High-Speed Sigma-Delta-Over-Fiber, IEEE Transactions on Microwave Theory and Techniques, vol. 67, no. 7, pp. 2861-2872, July 2019
<https://ieeexplore.ieee.org/document/8678474>
- 4) S. Kumagai et al.: Experimental Trials of 5G Ultra High-Density Distributed Antenna Systems, 2019 IEEE 90th Vehicular Technology Conference (VTC2019-Fall), pp.1-5, 2019
- 5) J. Pang et al.: A 28-GHz CMOS Phased-Array Beamformer Utilizing Neutralized Bi-Directional Technique Supporting Dual-Polarized MIMO for 5G NR, IEEE Journal of Solid-State Circuits, vol. 55, no. 9, pp.2371-2386, September 2020
<https://ieeexplore.ieee.org/document/9102243>
- 6) Evolved Universal Terrestrial Radio Access (E-UTRA); Physical channels and modulation, version 10.7.0: 3GPP TS 36.211, February 2013
https://www.arib.or.jp/english/html/overview/doc/STD-T104v2_20/5_Appendix/Rel10/36/36211-a70.pdf
- 7) M. Hayakawa, T. Mochizuki, M. Hirabe, T. Kikuma and D. Nose: Effect of Nonlinear Distortion and Null Stability on Spatial-multiplexing Performance using 4.65-GHz-Band Active Antenna System with DPD, 2019 49th European Microwave Conference (EuMC), pp.1076-1079, October 2019
<https://ieeexplore.ieee.org/document/8910751>
- 8) T. Kuwabara, N. Tawa, Y. Maruta, S. Hori and T. Kaneko: A 39 GHz MU-MIMO using 256 Element Hybrid AAS with Coherent Beam-Forming for 5G and Beyond IAB Applications, 2021 51st European Microwave Conference (EuMC), pp.580-583, April 2022
<https://ieeexplore.ieee.org/document/9784205>
- 9) NR; Physical channels and modulation, version 15.4.0: 3GPP TS 38.214, December 2018
- 10) E. Bjornson, Jakob Hoydis, and Luca Sanguinetti: Massive MIMO Networks: Spectral, Energy, and Hardware Efficiency, Now Publishers, 2017

Authors' Profiles

TAWA Noriaki

Professional
Wireless Access Development Department

KUWABARA Toshihide

Senior Professional
Wireless Access Development Department

MARUTA Yasushi

Senior Professional
Wireless Access Development Department

KANEKO Tomoya

Senior Professional
Wireless Access Development Department

Information about the NEC Technical Journal

Thank you for reading the paper.

If you are interested in the NEC Technical Journal, you can also read other papers on our website.

Link to NEC Technical Journal website

Japanese

English

Vol.17 No.1 Special Issue on Open Network Technologies

– Network Technologies and Advanced Solutions at the Heart of an Open and Green Society

Remarks for Special Issue on Open Network Technologies
NEC's Technological Developments and Solutions for Open Networks

Papers for Special Issue

Open RAN and Supporting Virtualization Technologies

Innovations Brought by Open RAN
Reducing Energy Consumption in Mobile Networks
Self-configuring Smart Surfaces
Nuberu: Reliable RAN Virtualization in Shared Platforms
vrAIn: Deep Learning based Orchestration for Computing and Radio Resources in vRANs

Wireless Technologies for 5G/Beyond 5G

NEC's Energy Efficient Technologies Development for 5G and Beyond Base Stations toward Green Society
Millimeter-wave Beamforming IC and Antenna Modules with Bi-directional Transceiver Architecture
Radio-over-Fiber Systems with 1-bit Outphasing Modulation for 5G/6G Indoor Wireless Communication
28 GHz Multi-User Massive Distributed-MIMO with Spatial Division Multiplexing
28 GHz Over-the-Air Measurements Using an OTFS Multi-User Distributed MIMO System
Comprehensive Digital Predistortion for improving Nonlinear Affection and Transceivers Calibration to Maximize Spatial Multiplexing Performance in Massive MIMO with Sub6 GHz Band Active Antenna System
Black-Box Doherty Amplifier Design Method Without using Transistor Models
39 GHz 256 Element Hybrid Beam-forming Massive MIMO for 8 Multi-users Multiplexing

Initiatives in Open APN (Open Optical/All Optical)

NEC's Approach to APN Realization — Towards the Creation of Open Optical Networks
NEC's Approach to APN Realization — Features of APN Devices (WX Series)
NEC's Approach to APN Realization — Field Trials
Wavelength Conversion Technology Using Laser Sources with Silicon Photonics for All Photonics Network
Optical Device Technology Supporting NEC Open Networks — Optical Transmission Technology for 800G and Beyond

Initiatives in Core & Value Networks

Technologies Supporting Data Plane Control for a Carbon-Neutral Society
NEC's Network Slicing Supports People's Lives in the 5G Era
Application-Aware ICT Control Technology to Support DX Promotion with Active Use of Beyond 5G, IoT, and AI
Using Public Cloud for 5G Core Networks for Telecom Operators

Enhancing Network Services through Initiatives in Network Automation and Security

NEC's Approach to Full Automation of Network Operations in OSS
Autonomous Network Operation Based on User Requirements and Security Response Initiatives
Enhancing Information and Communications Networks Safety through Security Transparency Assurance Technology
Enhancing Supply Chain Management for Network Equipment and Its Operation

Network Utilization Solutions and Supporting Technologies

Positioning Solutions for Communication Service Providers
The Key to Unlocking the Full Potential of 5G with the Traffic Management Solution (TMS)
Introducing the UNIVERGE RV1200, All-in-one Integrated Compact Base Station, and Managed Services for Private 5G
Vertical Services Leveraging Private 5G to Support Industrial DX
Integrated Solution Combining Private 5G and LAN/RAN

Global 5G xHaul Transport Solutions

xHaul Solution Suite for Advanced Transport Networks
xHaul Transformation Services
xHaul Transport Automation Solutions
Fixed Wireless Transport Technologies in the 5G and Beyond 5G Eras
SDN/Automation for Beyond 5G
OAM Mode-Multiplexing Transmission System for High-Efficiency and High-Capacity Wireless Transmission

Toward Beyond 5G/6G

NEC's Vision and Initiatives towards the Beyond 5G Era

NEC Information

2022 C&C Prize Ceremony



Vol.17 No.1
September 2023

Special Issue TOP